

Advanced Sustainable Trilayer Cellulosic “Paper Separator” Functionalized with Nano-BaTiO₃ for Applications in Li-Ion Batteries and Supercapacitors

Mononita Das, Pradip Sekhar Das, Nimai Chand Pramanik, Rajendra Nath Basu, and Mir Wasim Raja*



Cite This: *ACS Omega* 2023, 8, 21315–21331



Read Online

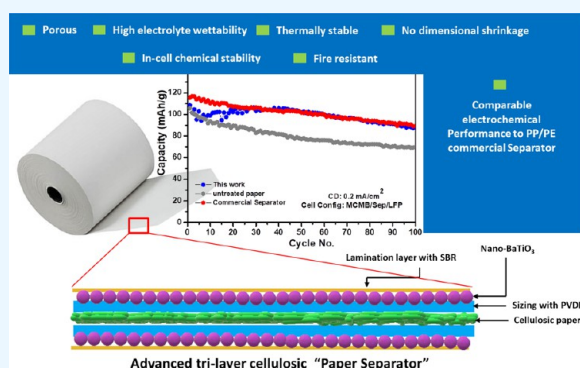
ACCESS |

Metrics & More

Article Recommendations

Supporting Information

ABSTRACT: In the quest of developing a sustainable, low-cost and improved separator membrane for application in energy storage devices like lithium-ion batteries (LIBs) and supercapacitors (SCs), here we fabricated a trilayer cellulose-based paper separator engineered with nano-BaTiO₃ powder. A scalable fabrication process of the paper separator was designed step-by-step by sizing with poly(vinylidene fluoride) (PVDF), thereafter impregnating nano-BaTiO₃ in the interlayer and finally laminating the ceramic layer with a low-concentration SBR solution. The fabricated separators showed excellent electrolyte wettability (216–270%), quicker electrolyte saturation, increased mechanical strength (43.96–50.15 MPa), and zero-dimensional shrinkage up to 200 °C. The electrochemical cell comprising graphite/paper separator/LiFePO₄ showed comparable electrochemical performances in terms of capacity retention at different current densities (0.05–0.8 mA/cm²) and long-term cycleability (300 cycles) with coulombic efficiency >96%. The in-cell chemical stability as tested for 8 weeks revealed a nominal change in bulk resistivity with no significant morphological changes. The vertical burning test as performed on a paper separator showed excellent flame-retardant property, a required safety feature for separator materials. To examine the multidevice compatibility, the paper separator was tested in supercapacitors, delivering a comparable performance to that of a commercial separator. The developed paper separator was also found to be compatible with most of the commercial cathode materials such as LiFePO₄, LiMn₂O₄, and NCM111.



1. INTRODUCTION

A separator in batteries is primarily used to isolate the anode and cathode to prevent electrical short circuit; simultaneously, it should also possess the ability of facile ionic transaction, high porosity and electrolyte wettability, lowered thickness, good mechanical strength, thermal stability, and intrinsic safety in abused conditions.^{1,2} Moreover, sustainability and cost are other two important techno-economic parameters that need to be addressed while developing separator materials. Achieving all these properties in a single material is indeed a challenging task.

Conventionally used microporous polyolefin (polypropylene/polyethylene)-based plastic separators have no doubt been a great commercial success in Li-ion batteries till date, but their low wettability towards commercial electrolytes, dimensional instability at elevated temperature, and environmental challenges due to plastic toxicity trigger the need for more advanced sustainable separators for lithium-ion batteries (LIBs).³ To mitigate these problems, two major approaches were undertaken: either surface modification of existing polyethylene (PE)/polypropylene (PP)-based separators⁴ or employment of other synthetic polymers, which include

poly(ethylene terephthalate) (PET) nonwovens,⁵ polyacrylonitrile (PAN),⁶ poly(vinylidene fluoride) (PVDF), etc.⁷

Besides these synthetic polymers, cellulose and/or its derivatives, e.g., bacterial cellulose,^{8,9} cellulose acetates,¹⁰ carboxymethyl cellulose,¹¹ cellulose nanofibers or nanocrystals,^{12,13} lignocellulose¹⁴ etc., have also been investigated widely as separator membranes. The obvious reasons for choosing cellulose as the separator material is definitely due to its sustainability, natural abundance, lower cost, and ease to compositionally modify or functionalize to achieve the desired properties as separator membranes in batteries. Moreover, unlike polyolefin, the cellulosic skeleton comprises hydroxyl and carbonyl groups, which can facilitate good interaction with carbonate electrolytes, enhancing its ability to soak a large amount of the electrolyte. Cellulose, having a higher initial

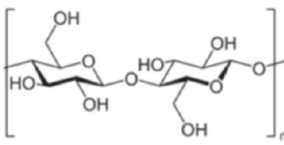
Received: April 26, 2023

Accepted: May 10, 2023

Published: May 29, 2023



Table 1. Comparison Chart on Different Types of Cellulosic Separators and Their Physicochemical and Electrochemical Properties



	Bacterial Cellulose <i>Huang et al. 8</i>	Cellulose Acetate <i>Xu et al. 10</i>	Cellulose Nanofiber <i>Kim et al. 12</i>	Cellulose nanocrystal <i>Gonçalves et al. 13</i>	Carboxyl methylcellulose <i>Kim et al. 11</i>
Thickness (μm)	25	20	33 \pm 2	150	34 \pm 4
Porosity (%), Gurley (s)	65	84.6	58 \pm 2	75	62 \pm 3
Wettability (%)	322	318	\geq 200	\geq 200	\geq 200
Thermal stability ($^{\circ}\text{C}$)	$>$ 300 $^{\circ}\text{C}$	-	150 $^{\circ}\text{C}$	-	$>$ 150 $^{\circ}\text{C}$
Mech. Strength (MPa)	-	56.2	56.2	Y:1860 \pm 180	-
Electrochemical Performance	140 $\text{mA}\cdot\text{g}^{-1}$; 89% retention after 100 cycles	148 $\text{mA}\cdot\text{g}^{-1}$; 89.5% retention after 50 cycles	123 $\text{mA}\cdot\text{g}^{-1}$; 94.31% retention after 100 cycles	120 $\text{mA}\cdot\text{g}^{-1}$ @ C/5	100 cycles @1C, Capacity 109.5 $\text{mA}\cdot\text{g}^{-1}$, 103.5 $\text{mA}\cdot\text{g}^{-1}$ (after 100 cycles), CD; 0.1C-5C
	Rice paper <i>Zhang et al. 22</i>	Tissue paper <i>Zeng et al. 15</i>	Pure Cellulose <i>Ly et al. 23</i>	Paper <i>Das et al. 17</i>	This work.
Thickness (μm)	100	45-55	35	65-70	20 \pm 5
Porosity (%), Gurley (s)	65	40-70	308s (Gurley)	15-25s (Gurley)	120 s (Gurley)
Wettability (%)	322	100-230	195	131-147	270.21
Thermal stability ($^{\circ}\text{C}$)	90 $^{\circ}\text{C}$ (- 0.26%)	200 $^{\circ}\text{C}$	300 $^{\circ}\text{C}$	$>$ 200 $^{\circ}\text{C}$	$>$ 200 $^{\circ}\text{C}$
Mech. Strength (MPa)	13.8	19.9	49	34.86–38.31	43.96-50.15 MPa
Electrochemical Performance	Comparable to Celgard @ 0.2 C, 1 C, and 2 C	Capacity retention 86.89% after 200 cycles	Capacity retention 91% after 100 cycles	Spec. Cap. 84.71-120.94 $\text{mA}\cdot\text{h}\cdot\text{g}^{-1}$ at 0.05 $\text{mA}\cdot\text{cm}^{-2}$; C.E. $>$ 97%; Current Density range: 0.1-0.4 $\text{mA}\cdot\text{cm}^{-2}$	300 cycles, C.E. $>$ 96%, Max. Current Density range 0.1-0.8 $\text{mA}\cdot\text{cm}^{-2}$, Spec. Cap. 117-133 $\text{mA}\cdot\text{h}\cdot\text{g}^{-1}$

decomposition temperature than that of polyolefin, can also impede dimensional collapse, ensuring the safety of the cells at elevated temperature. It is worthy to mention here that all of the previously reported results on cellulosic separators distinctly showed a significant improvement in terms of electrolyte wettability, thermochemical and dimensional stability, compatibility with Li-metal anode, and intrinsic safety against fire.

Recently, extensive research was carried out on cellulosic papers to use as separator materials in LIBs.^{15,16} However, pristine cellulosic paper with anisotropic pore distribution, large relative pore size, and poor mechanical strength has limited potential to be used as a separator in LIBs or other energy storage devices because of its undesired self-discharge phenomena and vital safety risks caused by lithium dendritic growth.¹⁵ Therefore, paper needs to be functionalized before its use in real cell environment.

Therefore, in the present research, an effort has been made to develop a trilayer ultrathin paper separator (will be henceforth referred as UTPS) using a scalable industry-friendly wet-coating method by functionalizing thin paper with polymers and ceramic nanoparticles. It is worthy to mention that the word “ultrathin” is used with respect to a previously developed paper-based separator in the authors’ lab,¹⁷ not in commercial comparison such as PP- or PE-based separators.

During the functionalization of the paper substrate, porosity and pore size were two major critical parameters that were duly optimized prior to application in cells. This is due to the fact that a large number of pores is essential in any separator material, but those need to be uniformly distributed to prevent dendritic growth of lithium during cycling and also to prevent the percolation of active electrode particles across the porous membrane.¹⁸ It is thus argued that the pore size of typical separator materials should be less than 1 μm .¹⁹ In this context, untreated paper (UP) does not qualify as a separator material to be used directly in the cells. Paper is an intrinsically porous material comprising large anisotropic pore spaces (ranging from 10 to 45 μm) originated from entangled cross-linked cellulosic fibers. Such high porosity may have an adverse impact on the electrochemical performance of the cells due to their poor mechanical strength and higher internal resistance. Keeping this in mind, in this study, the pore spaces present in untreated paper substrate have been systematically manipulated to fabricate a paper separator and to do that, the pristine paper has been coated with cellulose compatible polymers, namely poly(vinylidene difluoride) (PVDF) and styrene-butadiene rubber (SBR), via a scalable (in roll form) wet-coating method. PVDF is a well-known fluoropolymer possessing valuable properties: relatively high melting point, high mechanical strength at elevated temperatures, chemical

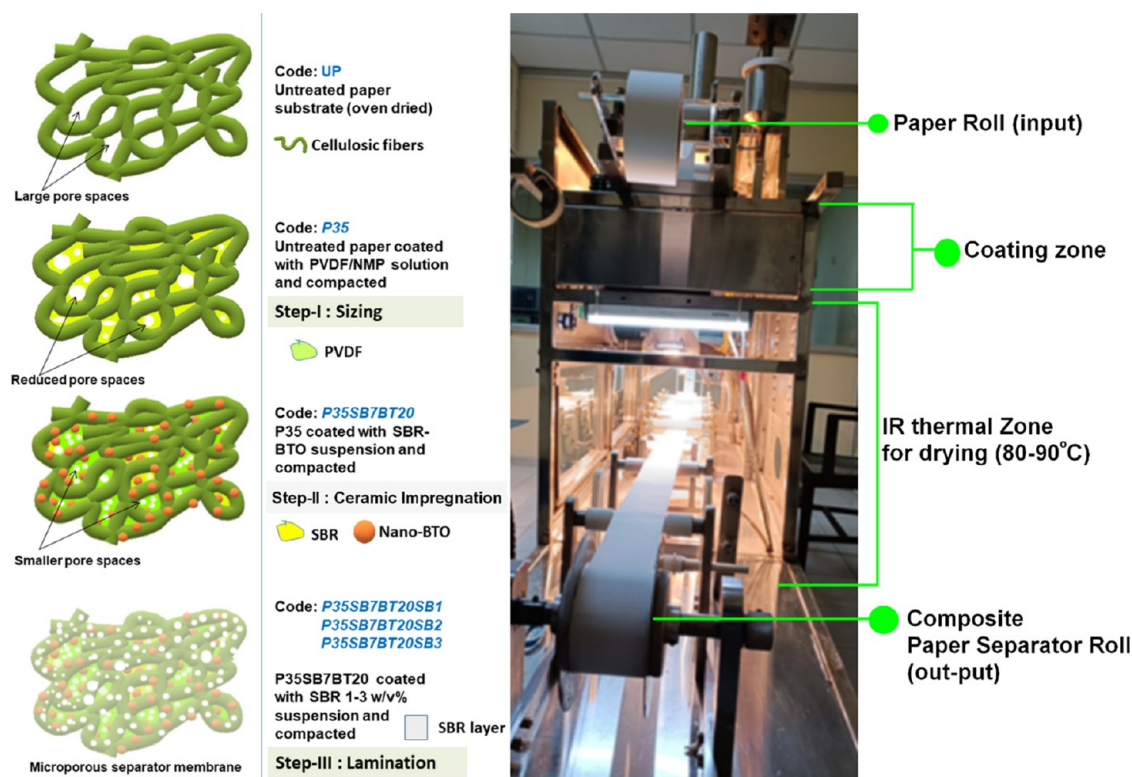


Figure 1. Schematic flow chart of the separator fabrication process involving sizing, ceramic impregnation, and lamination steps along with sample codes; the right-hand side shows the real image of an in-house-designed semiautomated double-decker composite paper separator fabrication machine.

resistance, resistance to hydrolysis, physiological inertness, low thermal conductivity, and exceptional resistance to ignition.²⁰ Furthermore, PVDF is widely used in paper-making industries as a sizing agent. On the other hand, ultrafine ferroelectric BaTiO₃ nanopowder was introduced here mainly as a filler material to enhance the structural integrity and thermal stability of the paper matrix. It is reported elsewhere that the presence of BTO may also facilitate electrolyte salt dissociation in charged species, can improve the ionic conductivity of the polymer used by increasing the amorphous content, and also enhance the lithium interface stability.^{21–23} The overall process of fabrication of a paper separator by the wet-coating method comprises three major processing steps: (i) sizing of the untreated paper substrate by PVDF, (ii) ceramic impregnation using BaTiO₃, and (iii) lamination by applying SBR coating. By optimizing these three process steps, a multilayer functionalized composite paper substrate was obtained, which after compaction using a calendaring machine resulted in an ultrathin paper separator.

The present research thus demonstrates a systematic study towards development of a technologically important low-cost sustainable paper-based separator component for energy storage devices like lithium-ion batteries (LIBs) and supercapacitors (SCs). A detailed discussion has also made here on the strategy of process scaling-up. The separators with varying polymer-ceramic compositions were fabricated and thoroughly characterized in terms of porosity, pore size distribution, microstructure, electrolyte wettability, thermal stability/shrinkage, mechanical behavior, and electrochemical performances both in lithium-ion cells and in supercapacitors. The chemical stability of the paper separator inside the lithium-ion full cell during calendar aging (without cycling) for 8 weeks

was evaluated using impedance spectroscopy (EIS) and surface imaging (FESEM and EDX) continuously. The combustion safety test was also carried out to evaluate the flame-retardant properties of composite paper separators. The obtained results were also duly compared with a commercial PP-based separator. The paper separators thus developed under this study might be considered a step toward achieving sustainability in the energy storage domain for both LIBs and supercapacitors. The current research status on cellulose and its derivatives as separator materials for LIBs is duly summarized in Table 1.

2. EXPERIMENTAL SECTION

2.1. Materials. Commercial cellulose paper was supplied from DSR AXYS Technology, India. Commercial PP-based separator was brought from MTI Corporation. Styrene butadiene rubber solution and BaTiO₃ nanopowder (Mol. wt. < 100 nm) were brought from Merck, Germany. Other battery chemicals such as commercial LiFePO₄, LiMn₂O₄, and NCM111 cathode powders, MCMC graphitic anode powder, PVDF powder, and commercial liquid electrolyte LiPF₆ in EC/DMC (1:2) were all purchased from MTI Corporation.

2.2. Fabrication of Paper Separator. The process of fabrication of UTPS has been carried out in three major steps: (i) sizing, (ii) ceramic impregnation, and (iii) lamination. The surface of paper is typically rough and inhomogeneous in nature; it is thus necessary to improve the surface properties by application of a suitable polymer. Here, the commercial cellulose paper (20 μm), named here as untreated paper (UP), was initially coated with 3.5 w/v % poly(vinylidene fluoride) (PVDF) in NMP solution via the wet-coating method using an in-house-fabricated double-decker (DD) coating machine

having in situ heating arrangement (80–90 °C), as shown in Figure 1.²⁴ Before coating with PVDF, the paper roll was demounted for 3 h at 80 °C in a vacuum oven. The dried PVDF-coated paper was then compacted using a calendaring machine under a load of 50–60 tons. This process is called surface “sizing”, which offers a certain benefit towards the large-scale fabrication process by improving the tensile strength of the thin paper substrate and extending the scope of further functionalization. The sizing process also consolidates the surface of the paper sheet, reducing its tendency to extricate surface fibers and moisture absorption under humid atmosphere.²⁵ Another most important role of this step is to reduce the pore spaces of the untreated bare paper substrate. Such minimization of pore spaces is required to offer directional penetration of electrolyte through the pores rather than fibers. The untreated paper coated with 3.5 w/v % PVDF thus obtained in this step will be henceforth termed as P35.

In the next step, the PVDF-coated paper was subjected to a second coating using an aqueous blend of styrene-butadiene rubber (SBR, 7.0 w/v %) and BaTiO₃ nano-ceramic powder (BTO, 2.0 w/v %) using the same wet-coating technique with the help of a DD fabricator machine. This step may be termed as “ceramic impregnation” or internal sizing using ceramic fillers. Through this process of internal sizing, several purposes are served. The surface energy of PVDF-coated paper becomes lowered.¹⁸ The ceramic filler BTO sits on the top surface of the fibers, giving reinforcement to the entangled cellulosic fibers of paper, and further pore spaces are reduced due to the SBR coating. Both the above two steps, i.e., surface sizing and ceramic impregnation steps, have a crucial impact on the wettability of the separator membrane. The paper separator at this functionalization stage will be henceforth termed as P35SB7BT20.

After two layers of successive coatings in the final step, the paper was further coated with an SBR aqueous solution of varying concentrations of 1.0–3.0 w/v %. This is called the “lamination” step. It provides a smooth separator surface, minimizes the pore spaces, and also works as a protective layer to impede the dissolution and/or leaching of ceramic particles in the electrolyte in the actual cell environment.

After the lamination step, the in situ-dried paper separator is finally compacted under a pressure of 20–30 tons using the calendaring machine. Depending on the concentration of SBR solution used for the lamination layer, the separators will be henceforth referred as P35SB7BT20SB1 (coated with 1.0 w/v % SBR), P35SB7BT20SB2 (coated with 2.0 w/v % SBR), and P35SB7BT20SB3 (coated with 3.0 w/v % SBR). The fabricated paper separators obtained at different stages (sizing, ceramic impregnation, and lamination) were kept for further characterizations. For better clarity, all of the experimental process steps are illustrated in Figure 1 along with their codes.

2.3. Characterization. The air permeability study of the separators fabricated with untreated paper (UP) and commercial polypropylene (PP) separator was carried out using a Gurley precision instrument (Model No. 4110N). A thickness gauge (Model no. CD-6” CSX, Mitutoyo Corp., Japan) was used to measure the thickness of the fabricated separators. The microstructural and morphological characterizations of the fabricated separators were conducted using a field emission scanning electron microscope (FESEM, Supra VP35 Carl Zeiss, Germany). The elemental composition of the fabricated separators was obtained by EDX analysis. The thermal behavior of the separators was studied by thermog-

ravimetric (TGA/DTA) analysis using a thermal analyzer (STA 449 F3 Jupiter, NETZSCH, Germany) under air atmosphere with a constant heating rate of 10 °C/min from room temperature (RT) to 700 °C. The thermal shrinkage of the separator samples along with the commercial separator was studied using a circular disk of diameter 15 mm. The membrane disks were placed inside a vacuum oven and the temperature was raised from RT to 200 °C at an interval of 25 °C, with a holding time of 10 min at each temperature. The dimensional changes of the separator specimen with respect to temperature were photographed.

A circular disk of diameter 15 mm of each separator sample was used to measure the electrolyte-soaking ability of fabricated and commercial separator membranes. The experiment was conducted inside an argon-filled glovebox (Braun, Germany). One drop (0.05 cm³) of standard electrolyte (1M LiPF₆) in ethylene carbonate (EC)/dimethyl carbonate (DMC) (1:2, w/w) was dropped on each of the circular separator samples and kept for 2 h. The spreading of liquid electrolyte on the separator surface was photographed. To quantify the electrolyte uptake capability of the fabricated and commercial separators, the following equation was used:²⁶

$$\frac{W_{\text{wet}} - W_{\text{dry}}}{W_{\text{dry}}} \times 100\% \quad (1)$$

where W_{dry} and W_{wet} are the respective separator weights before and after absorption of the liquid electrolyte. The contact angle measurement was carried using Data Physics OCA 15PRO, Germany, for the developed paper separators and commercial PP separator. The mechanical properties of the fabricated and commercial separators were measured by the Universal Testing Machine (Model No. 5500R, INSTRON, U.K.). The tensile stress and strain of the samples were measured both in machine direction (MD) and transverse direction (TD) with a crosshead speed of 10 mm/min and a load cell of 1 kN.

The bulk resistances of the electrolyte-soaked paper separators were measured by electrochemical impedance spectroscopy using Metrohm AutoLab, PGSTAT12/30, Netherlands, in the frequency range of 1 mHz to 1 MHz at room temperature. The separators were first soaked with liquid electrolyte (LiPF₆ in EC/DMC in 1:2 ratio) and sandwiched between two stainless steel (SS) electrodes of diameter 16 mm and crimped into 2032 coin-type cells inside the glovebox. The high-frequency intercept value on the Z' axis in the EIS plot was used to estimate the bulk resistance of the fabricated separators.

The electrochemical working potential window of the fabricated separator was estimated using 2032-type coin cells with the configuration Li/Separator/SS using an AutoLab PG-Stat instrument. Cell performances of the fabricated separators were studied in 2032-type coin cells using commercial-grade LiFePO₄ as the cathode (MTI) coated on aluminum film, MCMB (mesocarbon microbeads) anode (Maxtiger, China) coated on copper foils, and standard LiPF₆ in EC/DMC as the electrolyte. To compare the electrochemical performances of the fabricated separators, 2032-type coin cells were also made with a commercial polyolefin separator membrane (PP) (sourced from Maxtiger, China) and untreated commercial paper (UP). The electrochemical cell performances were examined by a BT2000 ARBIN automated battery tester

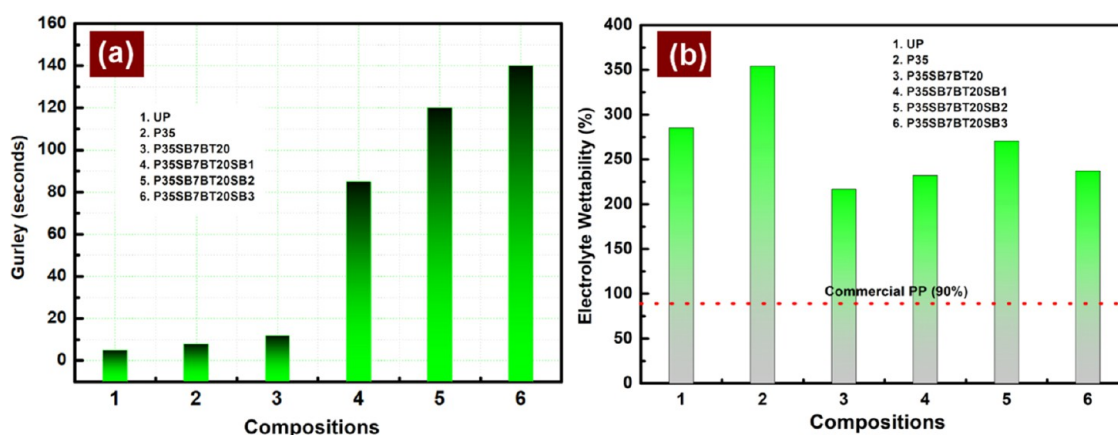


Figure 2. (a) Air permeability values in terms of Gurley seconds (per 100 cm³ air) of untreated paper and fabricated paper separators; (b) comparison of the electrolyte wettability of untreated paper and fabricated separators with commercial PP (red dotted line).

(ARBIN USA instrument) in the potential range of 2.5–3.8 V at different current densities ranging from 0.05 to 0.8 mA/cm².

The electrochemical performance of the developed separator (P35SB7BT20SB2) was studied to explore the application potentials in supercapacitors. Two cylindrical-type supercapacitors (SCs, labeled as N1-SC-UTPS and N2-SC-UTPS) of cell size 16 mm (ϕ) \times 36 mm (H) were fabricated and tested at C-MET (Thrissur, India) by using their state-of-the-art supercapacitor cell fabrication facility. Two wire-leaded carbon aerogel-based electrodes (aerogel carbon casted onto a thin aluminum foil current collector) with UTPS of optimized composition were used for this purpose. Two active electrodes and two layers of the separator (UPTS) were assembled as per the EDLC configuration; then, they were co-axially wound using a semiautomatic capacitor winding machine. After degassing the electrode wounds at 60 °C under vacuum, liquid electrolyte (1.0 M Et₄NBF₄ in propylene carbonate) was impregnated within the electrode wounds, which were then immediately sealed in aluminum cans of size 16 mm (ϕ) \times 36 mm (H). The electrochemical characteristics (cell capacitance and cell ESR) of the SCs thus made with UTPS were tested as per IEC 62391-1 (Class-I: energy storage and Class-II: power/surge power application). The constant current charge–discharge and constant current pulsing techniques were used for evaluating the cell capacitance (C_{eff}) and cell ESR, respectively, with a supercapacitor testing system. The charge–discharge cycling for SCs was done between 0.10 and 2.50 V DC, and the C_{eff} of the SCs was calculated from the discharge line of the charge–discharge curves using the following expanded equation:²⁷

$$C_{\text{eff}}(\text{Farad}) = \frac{I_d \times \Delta t}{\Delta V} = \frac{I_d \times (t_2 - t_1)}{(V_1 - V_2)} \quad (2)$$

where C_{eff} is the cell capacitance in farad, I_d (ampere) = discharge current, V_1 (volt) = 80% of V_R (V_R = upper rated voltage, 2.50 V DC), V_2 (volt) = 20% of V_R , and Δt (seconds) = $(t_2 - t_1)$ = time taken to discharge a charged SC from V_1 to V_2 . Similarly, the cell ESR was measured by applying five consecutive current pulses of 200 mA each sequentially for 10 ms on the SC, charged at V_R (2.50 V DC), and the cell ESR of SCs was calculated as²⁷

$$\text{ESR}_{\text{cell}}(\text{Ohm}) = \frac{\Delta V_{\text{pulse}}}{n \times I_{\text{pulse}}} \quad (3)$$

where ΔV_{pulse} is the drop of voltage due to the applied current pulse (I_{pulse}) and n is the number of consecutive pulses.

The stability inside the cell environment during aging was examined by fabricating 2032-type coin cells using paper separators, a standard MCMC anode, LiPF₆ in EC/DMC electrolyte, and LiFePO₄ cathode. The cells were aged for eight weeks without cycling at ambient temperature and EIS measurement was carried out at regular intervals of one week. To study the topology of the composite separator surfaces facing the anode and cathode sides, the aged cells were dismantled and FESEM images were taken. The elemental composition of the separator surfaces was studied using selected-area EDX mapping.

To explore the fire-retardant characteristics of the developed paper separator and PP, the vertical burning test (VBT) was performed and the separator was classified under UL 94 V ratings (V-0, V-1, and V-2).²⁸ This particular test measures the self-extinguishing time of the vertically oriented separator specimens. The test evaluates both the burning pattern, times and also the dripping of the burning specimen. Before conducting this flame test, the paper separators and PP were soaked in the electrolyte (LiPF₆ in EC/DMC) for 2 h and then exposed to a flame (source: gas lighter), and the changes were photographed with time.

3. RESULTS AND DISCUSSION

3.1. Air Permeability and Electrolyte Wettability.

Figure 2a shows the air permeability values of UP, P35, P35SB7BT20, and other fabricated paper separators (P35SB7BT20SB1, P35SB7BT20SB2, and P35SB7BT20SB3). Estimation of the air permeability of the separator membrane in terms of Gurley values (in seconds) is considered to be one of the critical characterization tools that helps to evaluate the nature of porosity and the homogeneous distribution of pores in the separator matrix. To perform this test, separator samples were cut into circular disks from different portions of the fabricated separators, particularly front, middle, and rear segments of the separator roll. The time required for permeation of 100 cm³ air through those samples was estimated in this test. As shown in Figure 2a, the untreated paper (UP) showed a very low Gurley value of 5s due to the presence of large-sized pore spaces. However, after completion of the first-layer coating (sizing) with PVDF 3.5 w/v %, the P35 separator showed a marginal increase in Gurley value (8

Table 2. Variation of the Values of BET Surface Area, Pore Volume, and Average Pore Diameters of Paper Separators w.r.t. SBR Content and Those of Untreated Commercial Paper, Analyzed by the N₂ Gas Sorption Technique at 77 K Using the BET Surface Area Analyzer (Nova 2000, Quantachrome)

sample code	description of sample	BET surface area (m ² /g)	total pore volume (cm ³ /g)	average pore diameter (nm)
P35SB7BT20SB1	sizing + ceramic impregnation + lamination: SBR 1.0% (w/v)	3.908	0.007	0.9
P35SB7BT20SB2	sizing + ceramic impregnation + lamination: SBR 2.0% (w/v)	4.771	0.010	1.0
P35SB7BT20SB3	sizing + ceramic impregnation + lamination: SBR 1.0% (w/v)	2.514	0.004	0.9
UP	commercial untreated paper	4.389	0.010	0.9

s). Thereafter, with the introduction of the SBR-BTO ceramic blend over P35, the Gurley value further increased to 12 s for P35SB7BT20. Upon the final coating with SBR (in the lamination step) with increased concentrations of 1–3 w/v %, Gurley values increased to 85 s (P35SB7BT20SB1), 120 s (P35SB7BT20SB2), and 140 s (P35SB7BT20SB3) respectively. The sharp increase in air permeability values revealed that the addition of polymeric layers (PVDF and SBR) during sizing, ceramic impregnation, and lamination processes has a significant effect toward reducing the number of pore spaces as well as their dimensions in the separator matrix. To quantitatively measure the porosity and pore diameter, the Brunauer–Emmett–Teller (BET) isotherm was also carried out for UP and other fabricated composite paper separators.

Figure 2b shows the variation of electrolyte (LiPF₆ in EC/DMC) wettability values of untreated paper and fabricated composite paper separators calculated using eq 1. The estimated values were also duly compared with the electrolyte wettability value of the commercial PP-based separator. The untreated cellulosic paper showed a wettability value of 285.29%, 3 times higher than that of the commercial PP (electrolyte wettability is 90%), due to its large number of pore spaces and also their high volumetric dimension. In the P35 separator, it was observed that PVDF coating significantly increased the hydrophobicity of the untreated paper substrate, which further enabled the cellulosic surface in a wide spreading of the organic liquid electrolyte and its faster adsorption process, resulting in a higher wettability value of 353.84%. In the next step, i.e., the ceramic impregnation process, further coating with SBR and BTO ceramic blend reduced the number of pore spaces that existed in the P35 surface, and also reduced its dimension, which was reflected in the decreased wettability value of 216.67% for the P35SB7BT20 separator. In the final lamination step, on coating the P35SB7BT20 separator with 1 w/v % SBR solution (P35SB7BT20SB1), the wettability value was found to increase marginally, reached a maximum value of 270.21% for the laminated separator using 2 w/v % SBR solution (P35SB7BT20SB2), and finally dropped to 236.95% for the P35SB7BT20SB3 separator laminated with 3 w/v % SBR. Although the lamination process was found to reduce the pore volume and pore dimension after the ceramic impregnation process, still, the electrolyte wettability values are significantly higher than those of the commercial PP separator membrane. This clearly suggests that the three-layer multistep coating process as executed on the untreated paper substrate had intrinsically increased the electrolyte-soaking ability of the developed composite paper separators.

3.2. Pore Characteristics. The pore characteristics of paper separators of different compositions were studied at 77 K by the nitrogen gas sorption technique using Brunauer–

Emmett–Teller (BET) surface area and a pore-size analyzer. Since adsorption–desorption is the surface phenomenon, the amount of gas adsorption depends on the surfaces, exposed to gas, size of pores and the partial pressure of the gas relative to its saturation pressure. Hence, the specific surface area of any porous materials can be measured by measuring the volume of gas adsorbed on its surfaces at a particular partial pressure, according to the well-known BET equation,²⁹

$$\frac{1}{w[(p_0/p) - 1]} = \frac{1}{w_m \times C} + \frac{C - 1}{w_m \times C \times (p_0/p)} \quad (4)$$

where p is the equilibrium pressure of the adsorbate, p_0 is the saturated equilibrium vapor pressure of the adsorbate, w is the weight of gas adsorbed at a relative pressure, w_m is the weight of adsorbate constituting a monolayer of surface coverage, and C is a constant, which is an indication of the magnitude of the adsorbent/adsorbate interactions. However, the BJH method is generally adopted to understand the distribution of pores within the matrix from the gas sorption isotherm data and calculate the average from there. A summary of the BET analysis, i.e., the specific surface area, total pore volumes, and average size of the pore, of different UTPS specimens and the commercial untreated paper, obtained from the N₂ sorption analysis, is given in Table 2.

It was observed that the pores in the paper separator matrix are in the microporous region; however, P35SB7BT20SB2 comprising 2.0% (w/v) of SBR possesses relatively larger pores of diameter 1.0 nm and has the highest pore volume of 0.010 cm³/g among the other two compositions (Table 1). This indicated that the process of sizing, ceramic impregnation, and lamination of the bare paper in the presence of polymeric moiety (PVDF and SBR) played a significant role in the pore characteristics, especially in the reduction of a number of pore spaces within the paper-based separator matrix. Further, it is important to mention here that the coating with different proportions of SBR on the outer surface enables the lamination with SBR, which significantly changes the pore characteristics of the top layer. When the SBR content increases further to 3.0 w/v %, it forms a compact lamination on the top surface and reduces the pore volume drastically to 0.004 cm³/g. Therefore, the study of these pore characteristics revealed that the polymeric layer formed by SBR at the top essentially laminates the inner components and enables the tuning of the entry of gas and/or liquid molecule into the core. The findings of the pore-characteristics study also are in good agreement with those of the air permeability (Gurley values) and also the electrolyte wettability (discussed below).

3.3. Contact Angle. Another most convincing method to assess the wettability is to measure the angle of contact between the probe liquid (water or electrolyte) and the surface

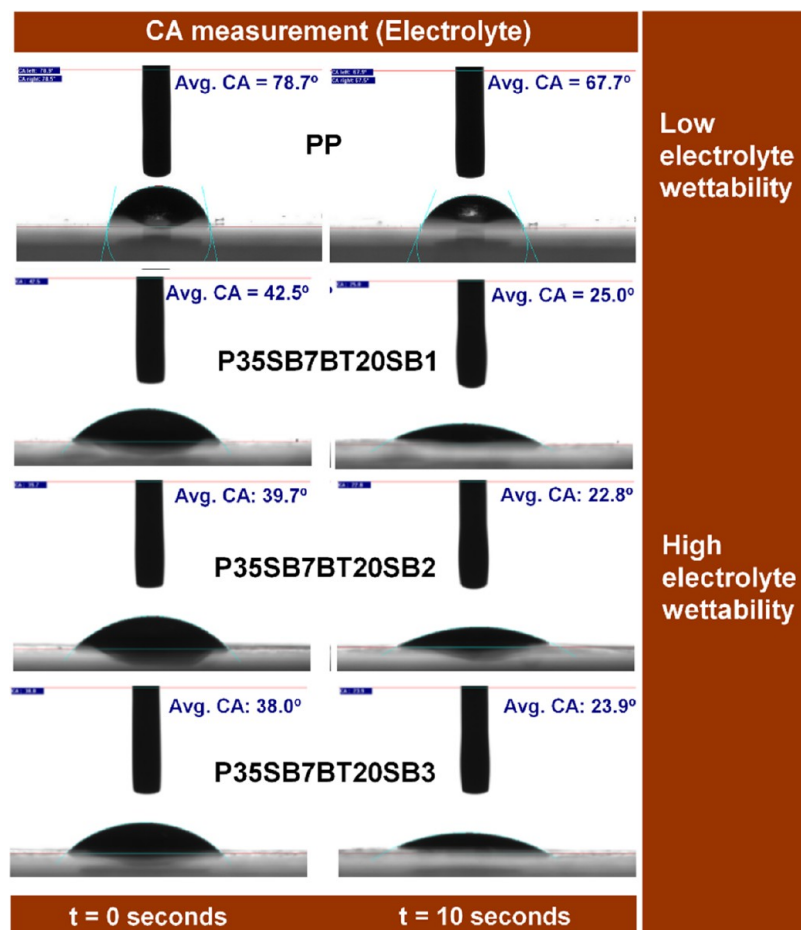


Figure 3. Contact angles measured using the standard electrolyte solution for (i) PP, (ii) P35SB7BT20SB1, (iii) P35SB7BT20SB2, and (iv) P35SB7BT20SB3 with respect to time.

of the paper substrate.³⁰ The variation of contact angles in terms of both the compositions of the developed paper separators and the probing liquids is presented in Figure 3 as well as in Figure S3. As shown in Figure S3, all of the fabricated separators P35SB7BT20SB1, P35SB7BT20SB2, and P35SB7BT20SB3 showed contact angles greater than 100° using water as the liquid, revealing the hydrophobic character of the paper surfaces. Such change from a hydrophilic cellulosic paper substrate to a hydrophobic cellulose-ceramic composite separator was achieved by PVDF coating during the process of sizing. However, in an electrochemical cell environment, the organic electrolyte will be in close contact with the separator surfaces; thus, it is good to test the contact angle of the developed separators using the standard electrolyte (LiPF₆ in EC/DMC) as the liquid. Figure 3 represents the time-dependent changes of contact angles in the electrolyte for the commercial PP-based separator as well as P35SB7BT20SB1, P35SB7BT20SB2, and P35SB7BT20SB3 paper separators. The laminated separators showed low contact angles ranging from 38.0 to 42.5° at the moment of dropping the electrolyte, which almost instantly reduced to 22–25° after 10 s, while the commercial PP-based separator showed a contact angle of 78.7° initially, which decreased to the value of 67.7° after 10 s duration. Such lower contact angles of the fabricated separators in comparison to the commercial one corroborate the findings obtained during estimation of electrolyte wettability. The

lowering of contact angle is basically related to the higher spreading of liquid on the substrate surface.

3.4. Microstructure. Microstructural imaging was carried out in every step of the fabrication process starting from untreated paper (UP) to the lamination step and is shown in Figure 4a–d. The untreated paper showed entangled cellulose fibers with heterogeneous porosity or pore spaces measuring 5–20 μm in length, as shown in Figure 4a. Thereafter, the surface sizing as done with the PVDF polymer resulted in a reduced number of pore spaces as well as pore dimension in the separator P35, as reflected in Figure 4b. From the micrograph of P35, it is also observed that the sized surface of paper was more compact (fiber density per unit volume) compared to the untreated paper (UP). In the step of ceramic impregnation, the porosity and pore diameter were found to be further reduced due to the introduction of SBR and BTO nanopowder, as seen in the micrograph presented in Figure 4c. A typical micrograph of the laminated paper separator P35SB7BT20SB2 as given in Figure 4d shows a significant reduction of pore spaces and increase in fiber compact density due to application of lamination coating with SBR. The EDX spectrum shown in Figure 4e, taken after the ceramic impregnation step for the fabricated separator P35SB7BT20, clearly indicates the presence of Ba, Ti, and O. It is interesting to see that untreated paper substrate is composed of several cellulosic fibers of different lengths and widths, as shown in Figure 4g. However, such fibers are not elementary in nature,

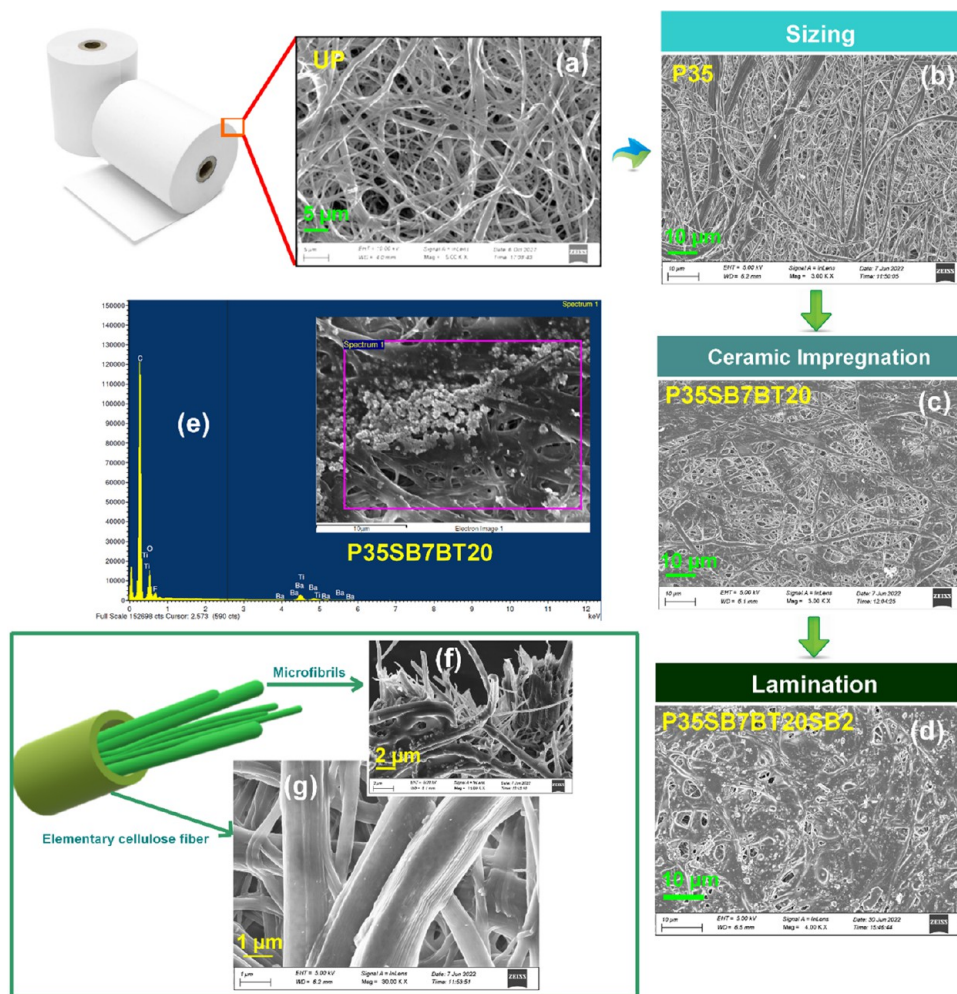


Figure 4. FESEM micrographs of (a) untreated paper (UP); (b) P35 separator obtained after sizing; (c) P35SB7BT20 separator after ceramic impregnation; (d) P35SB7BT20SB2 separator after laminating with 2 w/v % SBR; (e) selected-area elemental mapping by EDX of the separator P35SB7BT20; (f) and (g) a schematic representation of cellulose fiber and its elementary microfibrils displayed along with FESEM images taken on a P35 sized separator.

but are rather composed of a bundle of a large number of microfibrils. The FESEM image taken at the torn edge of the fabricated P35SB7BT20 separator as shown in Figure 4f revealed the presence of cellulose microfibrils. The ceramic nanoparticles were also found on the surface of the microfibrils. Thus, it can be stated that the ceramic impregnation step not only changed the surface properties but also the ceramics went to the surface of the elementary fibers, which might be helpful in strengthening the mechanical properties of the composite paper separator.

3.5. Mechanical Properties. The tensile properties of the separator are important from the cell manufacturing point of view, wherein the separator has to endure a certain tension of the winding machine during cell assembly.^{31,32} Figure 5a,b shows the load vs extension plot of untreated paper (UP), and P35SB7BT20SB1, P35SB7BT20SB2, and P35SB7BT20SB3 paper separators both in (a) machine direction and (b) transverse direction. The mechanical properties as obtained are summarized in Table S2. It revealed that the functionalization of paper separators using the duo-polymer and ceramics caused a marginal increase in their tensile stress at maximum load (43.96–50.15 MPa) compared to untreated paper substrate (46.26 MPa); however, 2-fold increase in tensile stress (paper separators: 26.57–28.21 MPa) was achieved in the transverse

direction (UP-TD: 11.83 MPa). A plot presenting the variation of tensile strengths both in machine direction (MD) and in transverse direction (TD) with respect to paper separator composition is shown in Figure S2 for better understanding. The increase in tensile strain as observed at maximum load both in MD and in TD might be due to the functionalization of the paper substrate. It is worthy to mention here that the mechanical properties of any paper-based material depend not only on the nature of the fiber but also on the bonding (H-bonding) between the fibers and its inherent strength.¹ Functionalization of the paper substrate with polymers and filler materials can thus have limited effect in enhancing the mechanical properties. However, if the coating polymers are able to create hydrogen bonding with the existing cellulose fibers of the paper substrate, an improvement in its mechanical property can be achieved. Therefore, the enhancement in mechanical properties in terms of tensile strain (MD and TD) in the fabricated paper separators was a combinational effect of both the nature of the cellulosic fibers present in the paper substrate and the inter- and intra-H-bonding created by the duo polymers (PVDF and SBR).

The dimensional change in elevated temperature was systematically studied using a circular disk of 19 mm diameter in an oven from 50 to 200 °C for UP, PP, and the fabricated

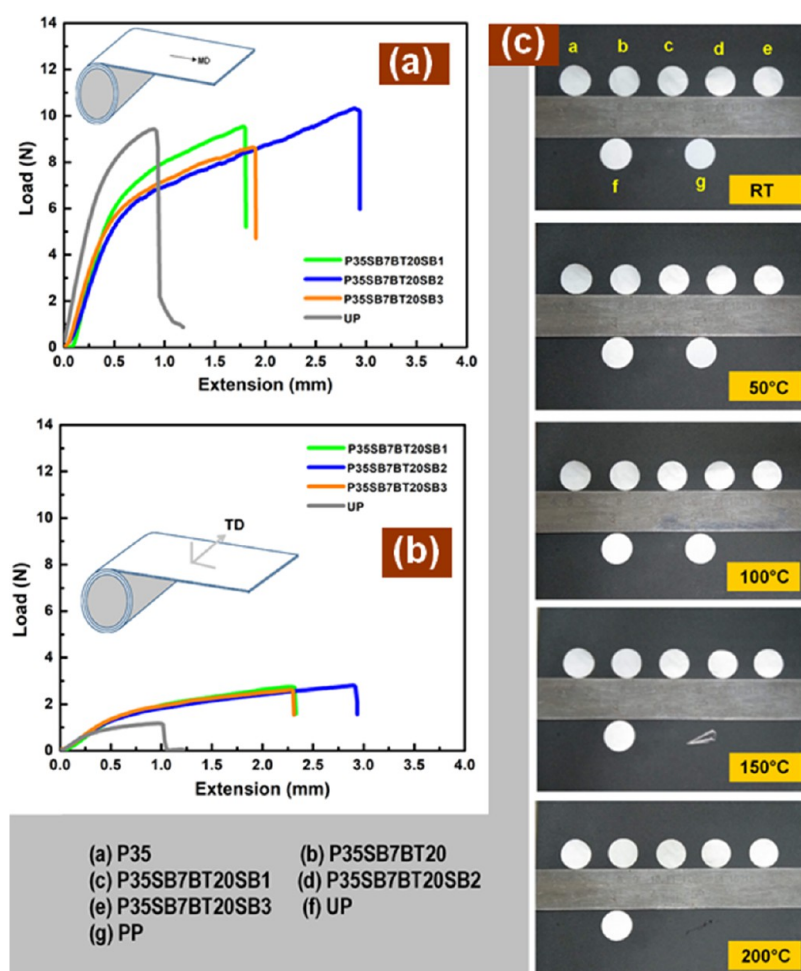


Figure 5. Load vs extension curve (a) in the machine direction (MD) and (b) in the transverse direction (TD). (c) Digital images of thermal shrinkage up to 200 °C for the separator specimen with code (a) P35, (b) P35SB7BT20, (c) P35SB7BT20SB1, (d) P35SB7BT20SB2, (e) P35SB7BT20SB3, (f) UP, and (g) commercial PP-based separator.

separators (P35, P35SB7BT20, P35SB7BT20SB1, P35SB7BT20SB2, and P35SB7BT20SB3). The changes in their dimension were photographed and are presented in Figure 5c. No dimensional shrinkage could be observed for the untreated paper and functionalized paper separators till 200 °C; however, the commercial PP membrane completely collapsed and melted to its transparent form at temperatures > 100 °C. This is due to the fact that heat can readily dissipate through the fibrous cellulosic network of the paper separator and ceramic filler materials can provide high thermal resistance. Apart from that, SBR also acts as a binder material to maintain the structural integrity of the separator at elevated temperatures. Thus, due to this improved thermal stability, fabricated paper separators can offer additional safety to the batteries by impeding short circuits in the thermally abused state.

For further analysis of thermal degradation from RT to 600 °C, TGA/DTA was performed for all of the fabricated paper separators and is shown in Figure S1. A sharp peak of major weight loss could be observed in the inset of Figure S1 for all of the paper separators at 321 °C, followed by two small weight losses at about 461 and 486 °C. The major weight loss was attributed to the removal of the surface and intrinsically H-bonded water molecules from the cellulosic matrix. The latter

peaks correspond to the thermal degradation of the polymers (PVDF and SBR) used as binders in the paper separators.

A summary of all physicochemical properties of the paper-based composite separators with variable compositions developed at different stages during processing with untreated paper is presented in Table S1.

3.6. Electrical and Electrochemical Performance.

3.6.1. Impedance Spectroscopy. EIS was carried out using 2032 coin-type symmetrical SS/separator/SS cells and the frequency-dependent impedance plots of the fabricated separators are shown in Figure 6a. All of the separators revealed straight-line profiles inclined towards the Z' axis, representing electrode–electrolyte double-layer capacitance behavior. The bulk resistance values of the fabricated separators were estimated from the high-frequency intercept of the Nyquist plot on the Z' axis and are presented in tabular form in the inset of Figure 6a. The effect of sizing, ceramic impregnation, and lamination was quite evident with the increase in resistance values of the fabricated paper separators: P35 (1.27 Ω), P35SB7BT20 (1.70 Ω), P35SB7BT20SB1 (4.23 Ω), P35SB7BT20SB2 (5.84 Ω), and P35SB7BT20SB3 (7.33 Ω). The surface sizing in P35 resulted in lower impedance value of 1.27 Ω due to the presence of comparatively greater number of pore spaces than the ceramic impregnated and laminated separators. Although ceramic impregnation of the

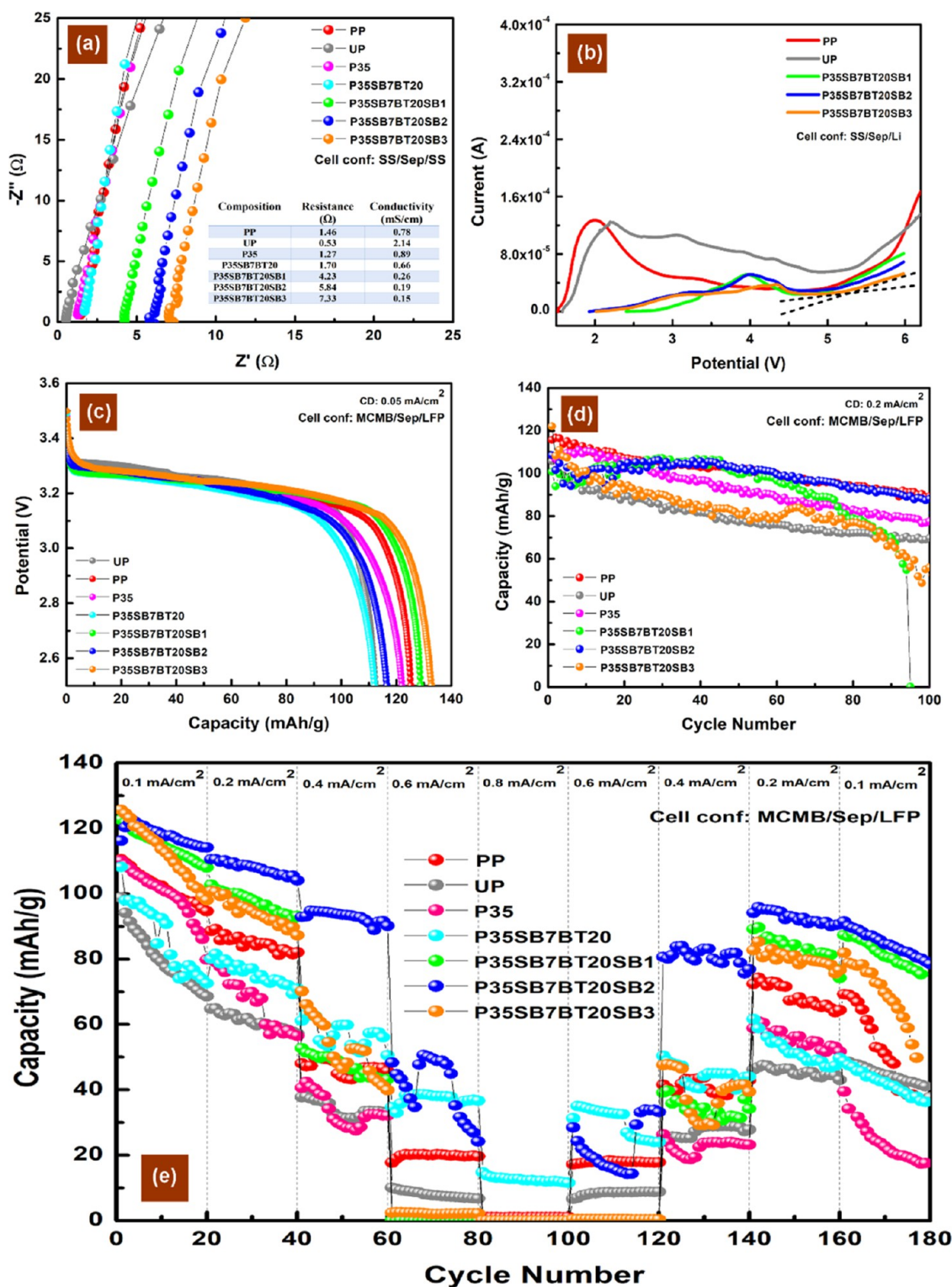


Figure 6. (a) Nyquist plot of fabricated paper separators; (b) electrochemical stability window of fabricated paper separators at a scan rate of 2.44 mV/s; electrochemical cell performance in 2032 coin-type cell fabricated with MCMB anode, LiPF₆ (EC/DMC) liquid electrolyte-soaked separators, and LiFePO₄ cathode; (c) initial charge–discharge profiles of UP and commercial PP along with fabricated separators; (d) cycleability plot at a current density of 0.2 mA/cm²; and (e) cycling performance of UP, P35, and fabricated separators at current densities in the range of 0.1–0.8 mA/cm².

separators by introducing the polymeric blend of the nano-ceramic powder (SBR and BTO) sacrificed few pore spaces in the P35 separator matrix, the presence of ceramics on the other side facilitated the wettability of the separator. Thus, the dual competing effect resulted in a marginal change in impedance

value in the P35SB7BT20 separator. In the laminated separators, i.e., P35SB7BT20SB1, P35SB7BT20SB2, and P35SB7BT20SB3, a large number of pores were sacrificed with the increasing concentration of SBR (conc. range 1.0–3.0 w/v %), resulting in higher impedance values. The

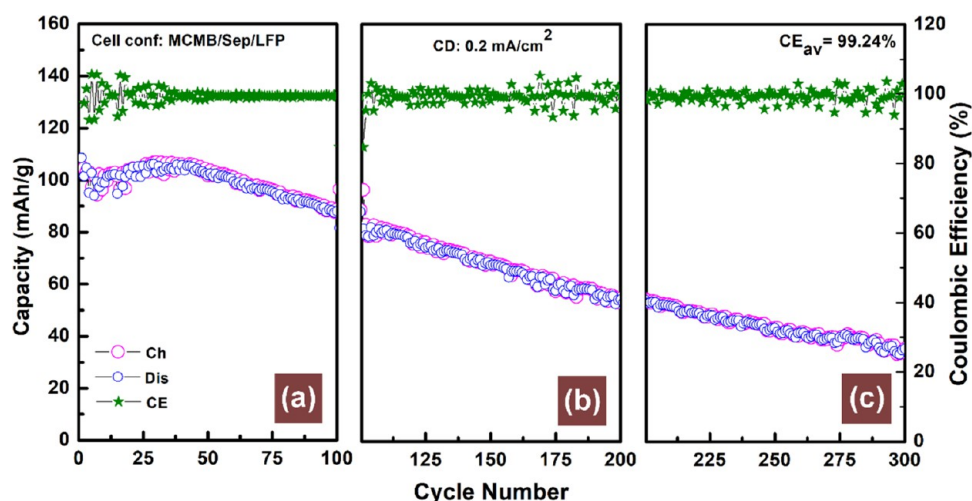


Figure 7. Capacity vs cycle number plot of the fabricated separator, P35SB7BT20SB2, up to 300 cycles. The Y axis represents the coulombic efficiency values in each charge–discharge cycle. Each plot from left to right represents the cycle numbers ranging from (a) 1st to 100th, (b) 101th to 200th and (c) 201th to 300th.

corresponding ionic conductivities of the electrolyte-soaked separators are also tabulated in the inset, reflecting a gradual decrease in ionic conductivities.

The EIS results in the summary suggested that the manipulation of pore spaces definitely has an adverse effect on the separator resistance and ionic conductivities; however, an optimization is necessary to achieve a balance between wettability and separator impedance values. In that respect, all of the paper separators might be qualified as good-quality working separators with acceptable porosity, wettability, and resistance.

3.6.2. Electrochemical Window. The working electrochemical windows for the paper separators were measured by the linear sweep voltammetry technique by scanning from OCV to 6 V at 2.44 mV/s scan rate. For this experiment, 2032-type coin cells with the cell configuration Li/Separator/SS using liquid electrolyte-soaked paper separators were fabricated. In the current vs potential plots shown in Figure 6b, small humps can be observed for all paper-based composite separators nearly at 4.0 V. This can be due to the formation of the passivation layer at the working electrode side. A sharp increase in current could be found above 5.1 V for the paper separators, which might be due to the decomposition of the liquid electrolyte. On the other hand, the working potential windows of the untreated paper (UP) and commercial plastic separator (PP) were found to be around 5.0 V from their LSV profiles in Figure 6b. Therefore, the working potential window as obtained for the paper separators was found to be nearly 5.1 V, which is suitable for almost every conventional commercial cathode material.

3.6.3. Electrochemical Full Cell Performance in LIBs. A comparison of the initial discharge profiles of 2032-type coin cells with a cell configuration of MCMB/separator/LiFePO₄ fabricated using untreated paper (UP), commercial PP, and fabricated paper separators is given in Figure 6c. Prior to cell fabrication, all of the separators were saturated with commercial standard LiPF₆ (EC/DMC-1:2) electrolyte for 2 h inside a glovebox. The specific discharge capacities of the cells were found to be 112 mAh/g (UP), 125 mAh/g (PP), 122 mAh/g (P35), 129 mAh/g (P35SB7BT20SB1), 117 mAh/g (P35SB7BT20SB2), and 133 mAh/g (P35SB7BT20SB13).

The cycling performance at 0.2 mA/cm² current density was studied for all of the fabricated separators, including UP and the commercial separator, PP. UP showed lower capacity values than PP and the fabricated separators. A comparable cycling performance to that of PP was obtained for the P35SB7BT20SB2 separator with a similar capacity retention up to 100 cycles. From Figure 6d, it is also found that both lower and higher concentrations (1.0 and 3.0 w/v %) of SBR used for lamination in P35SB7BT20SB1 and P35SB7BT20SB3 separators could not perform well in the cycling test. This might be due to the fact that a lower SBR concentration might not be sufficient to laminate the separator matrix homogeneously, whereas a high SBR concentration of 3.0 w/v % suffered from uneven lamination coating along with polymeric segregation on the separator surface, leading to exposure of the ceramic layer. An interesting result was found when the cells were cycled at increasing current densities from 0.1 to 0.8 mA/cm² and thereafter, reversing back to the initial current density (shown in Figure 6e). All laminated separators (P35SB7BT20SB1, P35SB7BT20SB2, and P35SB7BT20SB3) delivered higher capacities at lower current densities than the untreated paper (UP), but failed to perform at a very high current density of 0.8 mA/cm² because of the impedance developed due to the lamination layer, resulting in hindrance of the Li-ion mobility across the separator membrane. On the contrary, the separator without lamination (P35SB7BT20) still produced some capacities at 0.8 mA/cm². The results corroborated the ionic conductivities found for different separator compositions. While reversing back to lower current densities, the laminated separator was found to recover the capacity better than the UP and nonlaminated paper separators (P35, P35SB7BT20). Figure 7 describes the long-term cycling behavior of the laminated P35SB7BT20SB2 separator at a current density of 0.2 mA/cm² up to 300 cycles, including the coulombic efficiency of the cell. The cell showed >95% coulombic efficiency throughout the cycling test.

3.6.4. Multicathode Compatibility and Elevated Temperature Performance in LIBs. To evaluate the multicathode compatibility, the developed composite paper separator (P35SB7BT20SB2) was tested in 2032-type coin cell configuration using the MCMB anode, standard electrolyte,

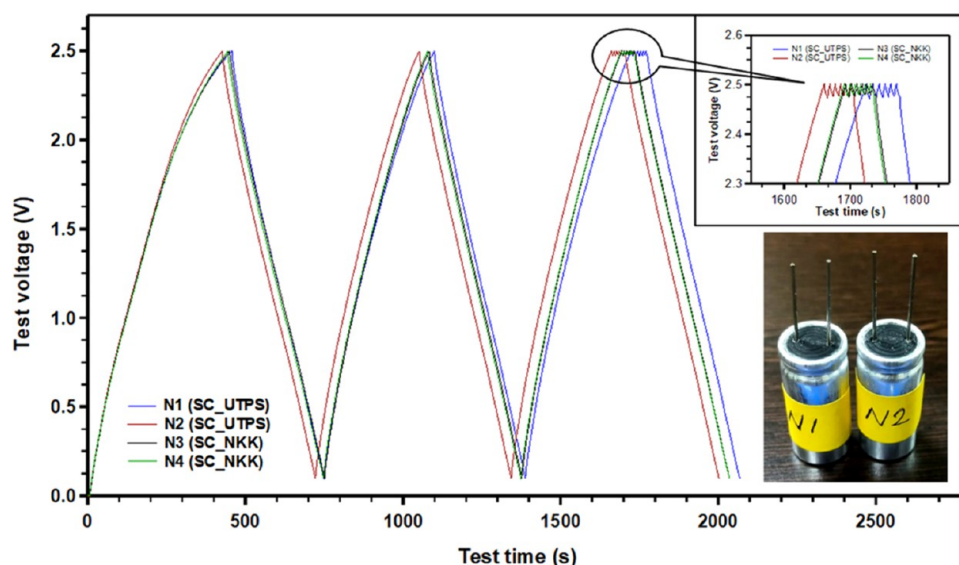


Figure 8. Typical constant current charge–discharge (CDC@260 mA) patterns of SCs, made with (a) the developed paper separator (N1-SC-UTPS and N2-SC-UTPS) and NKK branded commercial paper separator (N3-SC-NKK and N4-SC-NKK), carried out as per IEC 62391-1 (Class-II) by using the supercapacitor testing system. The inset represents the enlarged portion of CDC patterns during the constant current pulsing stage for measuring the cell ESR of SCs.

and three different commercial cathodes, namely LiFePO_4 (LFP), LiMn_2O_4 (LMO), and $\text{LiNi}_{1/3}\text{Co}_{1/3}\text{Mn}_{1/3}\text{O}_2$ (NCM111). Their typical charge–discharge profiles are presented in Figure S4. It was found that the composite paper separator delivered a specific discharge capacity of 114.66 mAh/g, 59.18 mAh/g, and 164.99 mAh/g with respect to LFP, LMO, and NCM111 respectively. The obtained capacity values were found to be well matched with their practical achievable capacities in Li-ion batteries. The capacity vs cycle number plots of MCMB/P35SB7BT20SB2/LMO and MCMB/P35SB7BT20SB2/NCM cells are presented in Figure S5. Both the cells were cycled at different current densities ranging from 0.1 to 1.2 mA/cm² for 20 cycles at each current density and their performance shows a good cycle retention of both electrodes with the designed separator.

In another attempt, the electrochemical cell performance at elevated temperatures for the optimized composite paper separator was evaluated from room temperature to 80 °C and duly compared with the cell performance of PP/PE-based commercial separators. Figure S6a demonstrates the performance of the commercial separator, which revealed that the plastic separator initially performed well up to 60 °C; however, at 80 °C, it showed false charging due to the dimensional degradation caused by intramolecular motion of polymeric moieties present in the plastic separator. On the other hand, the paper-based composite separator (P35SB7BT20SB2) showed satisfactory cycling at 80 °C (Figure S6b). These results further corroborated the intrinsic integrity of the composite separator at elevated temperature in a real cell environment.

3.6.5. Electrochemical Performance in Supercapacitors. The charge–discharge patterns of the SCs thus fabricated using UTPS were found to be identical and are highly reversible, which indicated no significant loss or deintegration of UTPS during the charge–discharge cycling. The C_{eff} and ESR_{cell} of the UTPS-based SCs were found to be in the range of 25.79 ± 0.2 F and 20.6 ± 0.3 m Ω . In order to compare the UTPS performance in of the SCs, two SCs were also fabricated

using two identical carbon aerogel-based active electrodes and a commercial cellulose-based paper separator (NKK brand, Japan) in a similar fashion (labeled as N3-SC_NKK and N4-SC_NKK) and they were also tested in a similar manner. The cell capacitances and ESR of the SCs made with NKK branded paper separator were found to be 26.1 ± 0.06 F and 13.2 ± 0.5 m Ω , respectively. The typical charge–discharge plot of SCs fabricated using UTPS and NKK branded commercial paper separator is shown in Figure 8, which clearly revealed that the newly developed paper separator (UTPS) is highly comparable to commercial products and possesses a high application potential for use as separator in a wide range of electrochemical energy storage systems including Li-ion batteries and supercapacitors.

3.6.6. Calendar Aging Test at Room Temperature. The chemical stability of the separator membrane inside a cell environment needs to be addressed to examine its performance for long-term cycleability. Inside the lithium-ion cell, both the surfaces of the separator are exposed to the LiPF_6 (EC/DMC)-based organic liquid electrolyte, different chemical constituents, and, of course, different redox environments (anodic and cathodic compartments) during cycling. Therefore, to observe the related changes in the microstructure, surface topology, and electrical properties of the separator, calendar aging in full-cell configuration (MCMB/Sep/LFP) has been studied here using impedance spectroscopy (EIS) and microscopic imaging (FESEM and EDX) techniques. In contrast to cycling aging, the results obtained in calendar aging can be helpful to interpret the mechanism of formation of passivation layers (SEI), and facts related to dissolution of electrode particles and the chemical stability of the separator membrane depending on the cell chemistries.

For this purpose, 2032-type coin cells were fabricated using the developed paper separator (P35SB7BT20SB2) in both full-cell (MCMB/Sep/LFP) and symmetrical cell (SS/Sep/SS) configurations and, thereafter, measuring their impedance at every one-week interval throughout the total duration of eight weeks without electrochemical cycling. At the end of the study

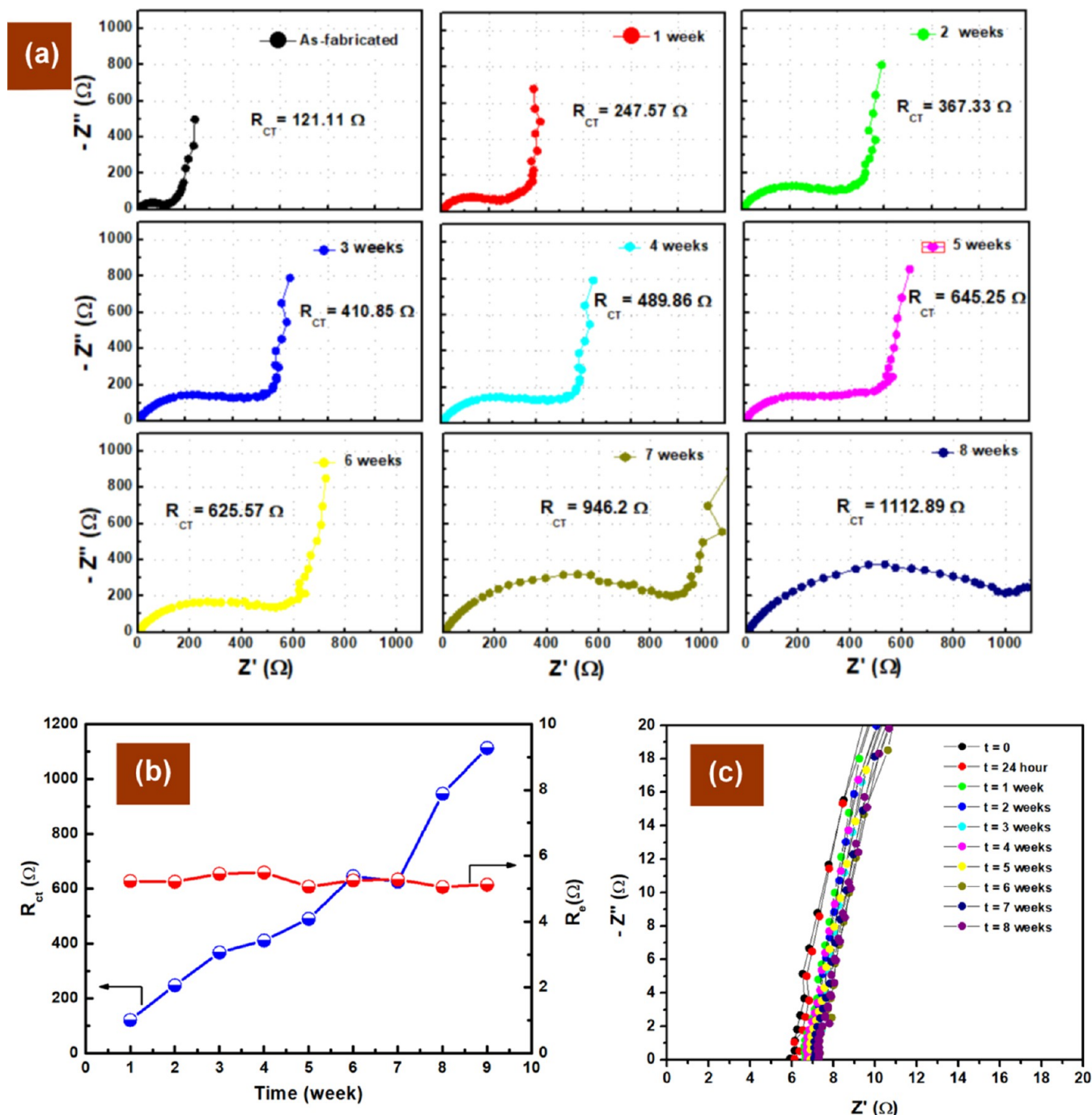


Figure 9. (a) Nyquist plot of the full cell (configuration: MCMB/Sep/LFP) fabricated with the paper separator P35SB7BT20SB2 during calendar aging (0–8 weeks); (b) time-dependent plot of electrolyte resistance (R_e) and charge transfer resistance (R_{ct}) of a symmetrical cell fabricated with the developed separator; and (c) Nyquist plot taken at regular intervals reflecting changes in the bulk impedance of the paper separator P35SB7BT20SB2 during calendar aging.

after eight weeks, the cells were dismantled and the separators were cleaned thoroughly several times with dimethyl carbonate (DMC) solvent to clear the soaked electrolytes. The surface properties of the separator membrane thus examined were compared with the separator that was dismantled just after 24 h of fabrication and cleaned in a similar way as stated earlier.

The Nyquist plots representing the time-dependent changes during aging in electrolyte resistance (R_e) and charge transfer resistance (R_{ct}) of the symmetrical cell fabricated with the developed separator are shown in Figure 9. It was observed

that the electrolyte resistance of the cell was found to be apparently constant (6–8 Ω) throughout the aging process, whereas the charge transfer resistance (R_{ct}) gradually increased over time. The R_{ct} value of the as-fabricated cell was found to be 121.11 Ω , which increased to a value of 1112.89 Ω after eight weeks. For better understanding, the results further plotted in Figure 9b,c show the changes in impedance values of the symmetric cell with respect to time. This suggests that the electrolyte resistance remained constant, where, due to side reactions and SEI formation, the charge transfer resistance

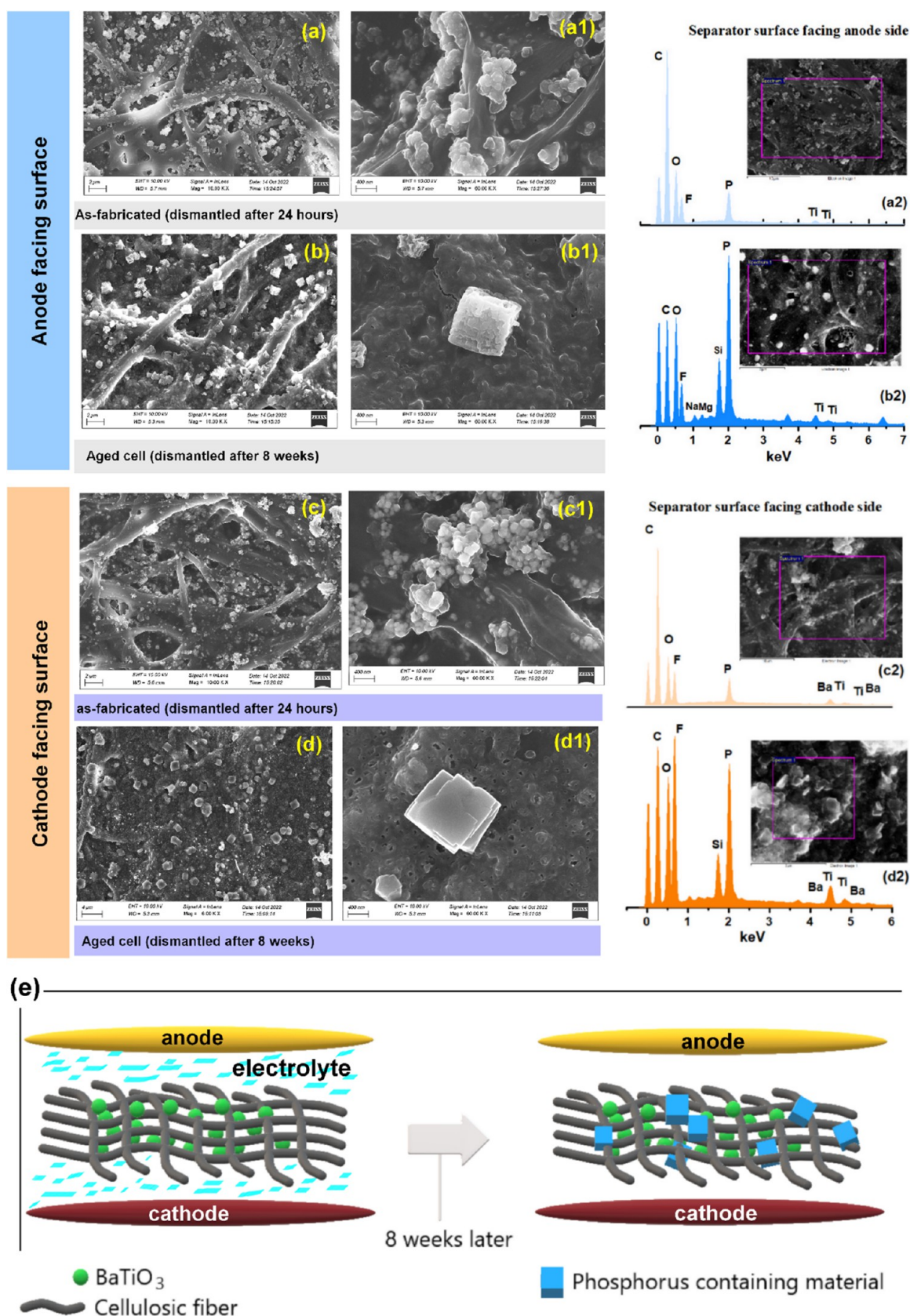


Figure 10. FESEM micrographs of the anode-facing surface of (a)-(a1) as-fabricated and (b)-(b1) aged cell dismantled after 8 weeks; FESEM micrographs of the cathode-facing surface of (c)-(c1) as-fabricated and (d)-(d1) aged separator after 8 weeks; corresponding selected-area EDX profile of anode-facing (a2-b2) and cathode facing surfaces (c2-d2) for both as-fabricated and aged separators; (e) a schematic illustration of phosphorus-containing material deposition on separator surfaces after aging.

increased to higher values. This further indirectly confirmed that ceramic particles embedded in the paper separator composite matrix might not be leaching out from the surface during aging; otherwise, incremental changes in electrolyte resistance might be observed due to dissolution of BTO particles in the electrolyte.

Robert et al. reported that separator morphology (PP-based) might be changed upon storage in a cell containing LiPF₆-EC-EMC electrolyte at elevated temperatures.³³ They argued that such changes may affect the lithium movement across the separator membrane due to blocking/covering of the pores of the separator, resulting in an increase in local ionic impedance. A nonuniform distribution of deposits originating from the liquid electrolyte was found in their study during aging of the full cell. In our case, we dismantled the aged cell after eight weeks, and both the surfaces of the aged paper separator (cathode-facing surface and anode-facing surface) were exposed under FESEM, followed by elemental analysis by EDX, as shown in Figure 10. The surface topology of the aged separator was duly compared with that of the nonaged separator dismantled after 24 h of assembly. The micrographs of separator surfaces for freshly dismantled cells after 24 h are shown in Figure 10a-a1,c-c1 for both anode- and cathode-facing surfaces; the morphology and microstructure looked apparently the same as the surface of the as-fabricated paper separator. However, cubic shaped particles could be found homogeneously deposited on both anode- and cathode-facing surfaces of the aged separator after eight weeks of calendar aging at RT, as shown in Figure 10b-b1,d-d1. To identify the elemental composition of the deposits on the paper separator surfaces, selected-area EDX was carried out on freshly dismantled separators and eight weeks' aged separators and is presented in Figure 10a2-b2,c2-d2. The EDX profiles for both anode- and cathode-facing surfaces of freshly dismantled and aged separators revealed the presence of phosphorus along with other known elements like C, O, Ba, Ti, F, and Si. The relative peak intensities of phosphorus were found to be increased on long-term aging. To probe this phenomenon, the EDX profile of the as-fabricated separator was compared and it was found that no phosphorus peak could be detected in the spectrum (refer to Figure 4e) of the as-fabricated paper separator. These observations indicated that phosphorus might be deposited on both anode- and cathode-facing surfaces of the aged composite paper separator due to decomposition of the electrolyte salt in the cell environment. The phosphorus-containing precipitate as found uniformly distributed on the separator might be one of the reasons for the capacity fading on long-term cycling of the cells. It is also envisaged that such depositions could be found on plastic PP/PE-based separators. Therefore, it is worthy to mention here that the reason for capacity fading on long-term cycling might not be correlated with the developed paper-based composite separator; rather, it is due to the degradation property of the liquid electrolyte during calendar aging. Such depositions may block the active pores of any such separator membrane, impeding Li-ion transport and, subsequently, capacity loss of the cell.

3.7. Flame Safety. The internal short circuit is one of the major causes of battery failure, fire hazards, and explosion. Short circuit (both internal and external) may lead to heat accumulation inside the cell, causing decomposition of the transition oxide cathodes, and subsequently release gaseous oxygen.^{34,35} Such phenomena may further result in oxidation of the electrolyte and separator in an exothermic fashion.

Therefore, both separators and liquid electrolytes have to play a significant role in preventing thermal runaway in LIBs. In our case, the functionalized composite paper separator was subjected to the IEC 60695-11-10 vertical flame standard test of combustion to measure its fire-retardant property. In our previous study, we observed that the commercial polypropylene-based separator comprising an aliphatic hydrocarbon backbone burnt itself rapidly without leaving any residual "char" under flame.¹⁷ The same is also reported in other studies also.³⁶ Here, we compared the effect of functionalization on resisting flame and/or combustion by comparing the nature of decomposition on exposure to flame for 10 s for both untreated paper and composite-functionalized paper separator (P35SB7BT20SB2). As demonstrated in Figure 11, the untreated paper was seen to catch fire readily

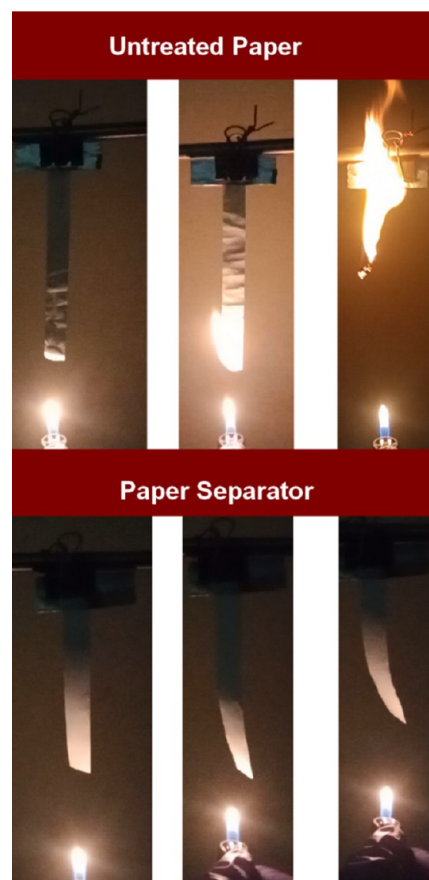


Figure 11. Digital images taken during the vertical flame test for both untreated (above) and functionalized paper separator (below).

under flame due to the intrinsic combustible nature of cellulose, whereas cellulose-ceramic composite paper separator interestingly remained flame resistive throughout the total exposure time. Therefore, as per the IEC 60695-11-10 vertical flame standard, the composite paper separator can be classified into V-0 ratings. Such flame-retardant properties will add extra safety features to the developed composite separator in real-time applications.

4. CONCLUSIONS

A sustainable, economic, and flexi paper-based composite separator was developed by functionalizing low-cost commercial paper by applying three critical processing steps: sizing,

ceramic impregnation, and lamination. The wet-coating method as designed to fabricate the paper separator was intrinsically simple, single-step, and industry-friendly. The developed microporous paper separators showed excellent wettability (216–270%) with quicker saturation to the commercial liquid electrolyte and no dimensional shrinkage up to 200 °C. The mechanical strength was found satisfactory to a value of 50.15 MPa in machine direction and 28.21 MPa in transverse direction. To establish the chemical stability of the developed paper-based composite separator in the organic electrolyte, calendar aging test was carried out, which showed no chemical degradation or ceramic leaching even after eight weeks of aging at room temperature. The electrochemical performance of the composite paper separator in full-cell configuration (MCMB/Sep/LFP) was found to be comparable to that of the commercial PP/PE-based plastic separator in terms of specific capacity, rate capability, coulombic efficiency (>95%), and long-term cycling performance (>300 cycles). To check multidevice compatibility, the developed separator was tested in supercapacitors as per the IEC 62391-1 (Class-II) method. The performance was found comparable to that of the commercial separator in terms of both effective capacitance (C_{eff}) and equivalent series resistance (ESR_{cell}). As per the IEC 60695-11-10 vertical flame standard, the developed composite paper separator was found to be flame retardant, a feature necessary in terms of safety aspects. The present research on the engineered flexible composite paper separator thus provides an opportunity to develop sustainable “better batteries” for future applications.

■ ASSOCIATED CONTENT

SI Supporting Information

The Supporting Information is available free of charge at <https://pubs.acs.org/doi/10.1021/acsomega.3c02859>.

Appendix A: Supplementary data compositions and related properties of different paper-based composite separators, thermal analysis of paper-based composite separators, variation in mechanical properties after functionalization, contact angle of the paper separators measured in water to indicate their hydrophobic nature, multicathode compatibility, elevated temperature performance of commercial and fabricated composite paper separator (PDF)

■ AUTHOR INFORMATION

Corresponding Author

Mir Wasim Raja – Energy Materials and Devices Division (Former Fuel Cell and Battery Division), CSIR-Central Glass and Ceramic Research Institute, Kolkata 700032, India; orcid.org/0000-0003-3090-7378; Phone: +91-33-2322-3393; Email: mwraja@cgcri.res.in

Authors

Mononita Das – Energy Materials and Devices Division (Former Fuel Cell and Battery Division), CSIR-Central Glass and Ceramic Research Institute, Kolkata 700032, India; orcid.org/0000-0003-2708-2504

Pradip Sekhar Das – Energy Materials and Devices Division (Former Fuel Cell and Battery Division), CSIR-Central Glass and Ceramic Research Institute, Kolkata 700032, India

Nimai Chand Pramanik – Advanced Materials & Chemical Characterization Division, CSIR-Central Glass and Ceramic Research Institute, Kolkata 700032, India

Rajendra Nath Basu – School of Advanced Materials, Green Energy and Sensor Systems, Indian Institute of Engineering Science and Technology, Howrah 711103, India

Complete contact information is available at:

<https://pubs.acs.org/doi/10.1021/acsomega.3c02859>

Author Contributions

M.D. fabricated the paper separator, and did data acquisition, analysis, plotting, and interpretation of the data. P.S.D. helped in fabrication, mechanical testing, and reviewing of the manuscript. N.C.P. analyzed the physical data and capacitor performance, and reviewed the manuscript. R.N.B. conceptualized the idea and design of the separator, and revised the manuscript critically for important intellectual content. M.W.R. conceptualized the idea and design of the separator, analyzed the data, prepared the figures/plotting, analyzed the cell performance data, and wrote the manuscript.

Funding

Financial support was received from the Department of Science & Technology, Government of India (DST, India), Sanction No. DST/TMD/MECSP/2 K17/07 (G) dated 10.05.2019.

Notes

The authors declare no competing financial interest.

■ ACKNOWLEDGMENTS

The authors are thankful to the Director, CSIR-Central Glass & Ceramic Research Institute, Kolkata, India, for her permission to publish this work. The authors acknowledge the extensive support received from CSIR, India (Council of Scientific & Industrial Research, India) to develop the paper-based separator as well as to design and fabricate an in-house-dedicated machine for scaling up the developed separators under CSIR-sponsored projects TAPSUN and FTT. The authors gratefully acknowledge the current financial support received from The Department of Science & Technology (DST), Government of India (DST, India), and also P. A. Abraham of the Centre for Materials for Electronics Technology (C-MET), Trissur for making supercapacitor cells with the optimized paper separator by using their state-of-art facilities and also testing the supercapacitors using the supercapacitor testing system as per IEC 62391-1 protocol.

■ REFERENCES

- (1) Li, A.; Yuen, A. C. Y.; Wang, W.; De Cachinho Cordeiro, I. M.; Wang, C.; Chen, T. B. Y.; Zhang, J.; Chan, Q. N.; Yeoh, G. H. A Review on Lithium-Ion Battery Separators towards Enhanced Safety Performances and Modelling Approaches. *Molecules* **2021**, *26*, 478.
- (2) Wu, H.; Chen, L.; Chen, Y. A Mini-Review of Advanced Separator Engineering in Lithium Metal Batteries. *Sustainable Energy Fuels* **2021**, *5*, 5656–5671.
- (3) Luo, W.; Cheng, S.; Wu, M.; Zhang, X.; Yang, D.; Rui, X. A Review of Advanced Separators for Rechargeable Batteries. *J. Power Sources* **2021**, *509*, No. 230372.
- (4) Wang, X.; Hu, Y.; Li, L.; Fang, H.; Fan, X.; Li, S. Preparation and Performance of Polypropylene Separator Modified by SiO₂/PVA Layer for Lithium Batteries. *e-Polymers* **2019**, *19*, 470–476.
- (5) Hao, J.; Lei, G.; Li, Z.; Wu, L.; Xiao, Q.; Wang, L. A Novel Polyethylene Terephthalate Nonwoven Separator Based on Electro-

- spinning Technique for Lithium Ion Battery. *J. Membr. Sci.* **2013**, *428*, 11–16.
- (6) Elia, G. A.; Ducros, J.-B.; Sotta, D.; Delhorbe, V.; Brun, A.; Marquardt, K.; Hahn, R. Polyacrylonitrile Separator for High-Performance Aluminum Batteries with Improved Interface Stability. *ACS Appl. Mater. Interfaces* **2017**, *9*, 38381–38389.
- (7) Liu, R.; Yuan, B.; Zhong, S.; Liu, J.; Dong, L.; Ji, Y.; Dong, Y.; Yang, C.; He, W. Poly(Vinylidene Fluoride) Separators for Next-generation Lithium Based Batteries. *Nano Select* **2021**, *2*, 2308–2345.
- (8) Huang, Q.; Zhao, C. Bacterial Cellulose Nanofiber Membrane for Use as Lithium-Ion Battery Separator. *IOP Conf. Ser.: Earth Environ. Sci.* **2021**, *647*, No. 012069.
- (9) Cheng, C.; Yang, R.; Wang, Y.; Fu, D.; Sheng, J.; Guo, X. A Bacterial Cellulose-Based Separator with Tunable Pore Size for Lithium-Ion Batteries. *Carbohydr. Polym.* **2023**, *304*, No. 120489.
- (10) Xu, P.; Zhang, D.; Shao, Z.; Chen, D. Cellulose Acetate-based Separators Prepared by a Reversible Acetylation Process for High-performance Lithium-ion Batteries. *J. Appl. Polym. Sci.* **2021**, *138*, 50738.
- (11) Kim, H.; Guccini, V.; Lu, H.; Salazar-Alvarez, G.; Lindbergh, G.; Cornell, A. Lithium Ion Battery Separators Based On Carboxylated Cellulose Nanofibers From Wood. *ACS Appl. Energy Mater.* **2019**, *2*, 1241–1250.
- (12) Kim, H.; Mattinen, U.; Guccini, V.; Liu, H.; Salazar-Alvarez, G.; Lindström, R. W.; Lindbergh, G.; Cornell, A. Feasibility of Chemically Modified Cellulose Nanofiber Membranes as Lithium-Ion Battery Separators. *ACS Appl. Mater. Interfaces* **2020**, *12*, 41211–41222.
- (13) Gonçalves, R.; Lizundia, E.; Silva, M. M.; Costa, C. M.; Lancers-Méndez, S. Mesoporous Cellulose Nanocrystal Membranes as Battery Separators for Environmentally Safer Lithium-Ion Batteries. *ACS Appl. Energy Mater.* **2019**, *2*, 3749–3761.
- (14) Bicy, K.; Mathew, D. E.; Stephen, A. M.; Royaud, I.; Poncot, M.; Godard, O.; Aranda, L.; Rouxel, D.; Kalarikkal, N.; Thomas, S. Sustainable Lithium-Ion Battery Separators Derived from Polyethylene Oxide/Lignocellulose Coated Electrospun P(VDF-TrFE) Nanofibrous Membranes. *Surf. Interfaces* **2022**, *29*, No. 101716.
- (15) Zeng, X.; Liu, Y.; He, R.; Li, T.; Hu, Y.; Wang, C.; Xu, J.; Wang, L.; Wang, H. Tissue Paper-Based Composite Separator Using Nano-SiO₂ Hybrid Crosslinked Polymer Electrolyte as Coating Layer for Lithium Ion Battery with Superior Security and Cycle Stability. *Cellulose* **2022**, *29*, 3985–4000.
- (16) Li, Z.; Wang, W.; Liang, X.; Wang, J.; Xu, Y.; Li, W. Fiber Swelling to Improve Cycle Performance of Paper-Based Separator for Lithium-Ion Batteries Application. *J. Energy Chem.* **2023**, *79*, 92–100.
- (17) Das, M.; Das, P. S.; Basu, R. N.; Raja, M. W. Cellulose-Ceramic Composite Flexible Paper Separator with Improved Wettability and Flame Retardant Properties for Lithium-Ion Batteries. *Cellulose* **2022**, *29*, 9899–9917.
- (18) Gören, A.; Costa, C. M.; Tamaño Machiavello, M. N.; Cíntora-Juárez, D.; Nunes-Pereira, J.; Tirado, J. L.; Silva, M. M.; Gomez Ribelles, J. L.; Lancers-Méndez, S. Effect of the Degree of Porosity on the Performance of Poly(Vinylidene Fluoride-Trifluoroethylene)/Poly(Ethylene Oxide) Blend Membranes for Lithium-Ion Battery Separators. *Solid State Ionics* **2015**, *280*, 1–9.
- (19) Deimede, V.; Elmasides, C. Separators for Lithium-Ion Batteries: A Review on the Production Processes and Recent Developments. *Energy Technol.* **2015**, *3*, 453–468.
- (20) Dallaev, R.; Pisarenko, T.; Sobola, D.; Orudzhev, F.; Ramazanov, S.; Trčka, T. Brief Review of PVDF Properties and Applications Potential. *Polymers* **2022**, *14*, 4793.
- (21) Vijaya Kumar Saroja, A. P.; Sundara, R. Barium Titanate-Based Porous Ceramic Flexible Membrane as a Separator for Room-Temperature Sodium-Ion Battery. *ACS Appl. Mater. Interfaces* **2019**, *11*, 3889–3896.
- (22) Zhang, L. C.; Sun, X.; Hu, Z.; Yuan, C. C.; Chen, C. H. Rice Paper as a Separator Membrane in Lithium-Ion Batteries. *J. Power Sources* **2012**, *204*, 149–154.
- (23) Lv, D.; Chai, J.; Wang, P.; Zhu, L.; Liu, C.; Nie, S.; Li, B.; Cui, G. Pure cellulose lithium-ion battery separator with tunable pore size and improved working stability by cellulose nanofibrils. *Carbohydr. Polym.* **2021**, *251*, No. 116975.
- (24) Raja, M. W.; Basu, R. N.; Pramanik, N. C.; Das, P. S.; Das, M. Paperator: The Paper-Based Ceramic Separator for Lithium-Ion Batteries and the Process Scale-Up Strategy. *ACS Appl. Energy Mater.* **2022**, *5*, 5841–5854.
- (25) Spagnuolo, L.; D’Orsi, R.; Operamolla, A. Nanocellulose for Paper and Textile Coating: The Importance of Surface Chemistry. *ChemPlusChem* **2022**, *87*, No. e202200204.
- (26) Gogia, A.; Wang, Y.; Rai, A. K.; Bhattacharya, R.; Subramanyam, G.; Kumar, J. Binder-Free, Thin-Film Ceramic-Coated Separators for Improved Safety of Lithium-Ion Batteries. *ACS Omega* **2021**, *6*, 4204–4211.
- (27) Conway, B. E. *Electrochemical Supercapacitors*; Springer US: Boston, MA, 1999. <https://doi.org/10.1007/978-1-4757-3058-6>.
- (28) *Flame Retardants*; Visakh, P. M.; Arao, Y., Eds.; Springer International Publishing: Cham, 2015. <https://doi.org/10.1007/978-3-319-03467-6>.
- (29) Brunauer, S.; Emmett, P. H.; Teller, E. Adsorption of Gases in Multimolecular Layers. *J. Am. Chem. Soc.* **1938**, *60*, 309–319.
- (30) Zhang, J.; Yue, L.; Kong, Q.; Liu, Z.; Zhou, X.; Zhang, C.; Xu, Q.; Zhang, B.; Ding, G.; Qin, B.; Duan, Y.; Wang, Q.; Yao, J.; Cui, G.; Chen, L. Sustainable, Heat-Resistant and Flame-Retardant Cellulose-Based Composite Separator for High-Performance Lithium Ion Battery. *Sci. Rep.* **2014**, *4*, No. 3935.
- (31) Li, Y.; Li, Q.; Tan, Z. A Review of Electrospun Nanofiber-Based Separators for Rechargeable Lithium-Ion Batteries. *J. Power Sources* **2019**, *443*, No. 227262.
- (32) Xing, J.; Li, J.; Fan, W.; Zhao, T.; Chen, X.; Li, H.; Cui, Y.; Wei, Z.; Zhao, Y. A Review on Nanofibrous Separators towards Enhanced Mechanical Properties for Lithium-Ion Batteries. *Composites, Part B* **2022**, *243*, No. 110105.
- (33) Bourlot, S.; Blanchard, P.; Robert, S. Investigation of Aging Mechanisms of High Power Li-Ion Cells Used for Hybrid Electric Vehicles. *J. Power Sources* **2011**, *196*, 6841–6846.
- (34) Liu, X.; Ren, D.; Hsu, H.; Feng, X.; Xu, G.-L.; Zhuang, M.; Gao, H.; Lu, L.; Han, X.; Chu, Z.; Li, J.; He, X.; Amine, K.; Ouyang, M. Thermal Runaway of Lithium-Ion Batteries without Internal Short Circuit. *Joule* **2018**, *2*, 2047–2064.
- (35) Sharifi-Asl, S.; Lu, J.; Amine, K.; Shahbazian-Yassar, R. Oxygen Release Degradation in Li-Ion Battery Cathode Materials: Mechanisms and Mitigating Approaches. *Adv. Energy Mater.* **2019**, *9*, No. 1900551.
- (36) Liao, C.; Wang, W.; Han, L.; Mu, X.; Wu, N.; Wang, J.; Gui, Z.; Hu, Y.; Kan, Y.; Song, L. A Flame Retardant Sandwiched Separator Coated with Ammonium Polyphosphate Wrapped by SiO₂ on Commercial Polyolefin for High Performance Safety Lithium Metal Batteries. *Appl. Mater. Today* **2020**, *21*, No. 100793.